Supplementary Information

Interfacial Modification between Argyrodite-type Solid-State Electrolytes and Li Metal Anodes using LiPON Interlayers

Jin Su*[ab], Mauro Pasta[ab], Ziyang Ning[ab], Xiangwen Gao[ab], Peter G. Bruce[ab] and Chris R.M. Grovenor*[ab]

[a]Department of Materials, University of Oxford, Parks Road, Oxford, OX1 3PH, UK

[b]The Faraday Institution, Quad One, Becquerel Avenue, Harwell Campus, Didcot, OX11 0RA, UK

Corresponding Authors

*E-mail: chris.grovenor@materials.ox.ac.uk; jin.su@materials.ox.ac.uk

Experimental Details

Preparation of argyrodite Li_6PS_5Cl SSE

Argyrodite Li_6PS_5Cl powder with a 325 mesh size (D50 ~ 10 µm) was purchased from AMPCERA. The Li_6PS_5Cl powder was pressed into 5 mm diameter pellets under a uniaxial pressure of 500 MPa, and the resulting pellets sintered at 300 °C for 10 min. This sintering process results in a reduced total resistance (as shown in Figure S1), probably because of the increased grain size in the bulk SSE, which is beneficial for both impedance reduction and Li ion migration through a microstructure with less interconnected porosity. All preparation processes were performed inside an Ar-filled glove box with $H_2O < 0.1$ ppm and $O_2 < 0.1$ ppm. LiPON layers with 30 nm thickness were deposited on the Li_6PS_5Cl pellet surface by radio magnetron (RF) sputtering from a Li_3PO_4 target at 2.5 W cm^{-2} powder density under a 0.6 Pa N_2 atmosphere at room temperature in a glove box. A 500 nm thick LiPON layer was deposited on a 100 nm Pt coated Si substrate by RF sputtering with the same conditions for measurement of the ionic conductivity of these thin LiPON films. A 100 nm Pt electrode was then deposited by RF sputtering under a 0.5 Pa Ar atmosphere with a power density of 2.5 W cm^{-2} to form a Pt/LiPON/Pt symmetric cell.

Characterization

X-ray diffraction (XRD) was conducted to confirm the crystalline structure of the Li_6PS_5Cl solid electrolyte pellets using a Rigaku Miniflex X-ray diffractometer with Cu $K\alpha_1$ radiation inside an Ar-filled glove box (O_2 and H_2O levels < 0.1 ppm). XRD patterns were obtained from 10° to 80° (2θ) using a step size of 0.01°. Fourier-transform infrared spectroscopy (FTIR) measurements were applied to confirm the chemical bonding states on the surface of the Li_6PS_5Cl pellets. FTIR was carried out in the attenuated total reflectance (ATR) mode using a Thermo Fisher Nicolet iS50 spectrometer over the wavenumber range of 500-4000 cm^{-1} with a 2 cm^{-1} resolution. X-ray photoelectron spectroscopy (XPS, PHI Versa Probe III) was carried out to analyse the chemical bonding state on surface of the Li_6PS_5Cl pellets. Survey and specific high-resolution spectra were obtained using a monochromatic Al Kα X-ray source. The binding energy of the C 1s peak at 284.8 eV was used for energy calibration. The XPS results were analyzed using CasaXPS software for chemical bond attribution and peak fitting. Scanning electron microscopy (SEM) images were obtained using a Thermo-Fisher Helios G4

CXe Plasma focused ion beam column (FIB)-SEM system. The Li_6PS_5Cl samples were mounted on a specimen stub and fixed into a vacuum transfer device for transfer from the glovebox to the Gatan vacuum transfer holder of the Plasma FIB to avoid air exposure. The electron and FIB ion beams aligned at 52° were confocal at a fixed sample working distance of 4 mm. To collect the FIB-SEM cross-section images, the sample stage was tilted so that the xenon plasma beam impacted vertically on the surface of the Li_6PS_5Cl pellet for the milling of trenches to allow cross-sectional imaging using ions accelerated to 30 kV. Energy-dispersive X-ray spectroscopy (EDX) scans were carried out by an Ultim Max 170 X-ray detector (Oxford Instruments) to obtain elemental maps. To investigate the wettability of LiPON coated Li_6PS_5Cl pellet, the Li metal on the LiPON coated Li_6PS_5Cl pellet was melted by holding at 200 °C for 10 min, and the molten Li spread out quickly and uniformly covering the surface of the LiPON coated Li_6PS_5Cl pellet.

Cell assembly and electrochemical characterization

500 nm thick Pt electrodes were deposited on both surfaces of the Li_6PS_5Cl pellets by RF sputtering under a 0.5 Pa Ar atmosphere with a power density of 2.5 W cm^{-2}, forming a Pt/Li_6PS_5Cl/Pt stack for ionic conductivity measurements using a mask with a 2 mm diameter aperture. Electrochemical impedance spectroscopy (EIS) measurements were carried out on the cells over the frequency range from 30 MHz to 1 Hz with a perturbation amplitude of 10 mV using a Biologic MTZ-35 impedance analyzer. The EIS data were analyzed using the ZView software. Ionic conductivities were calculated using $\sigma = d/(RA)$, where R is the total resistance of Li_6PS_5Cl ceramic pellet taken from the real axis on the Nyquist plot, d is the thickness of the pellet, and A is the area of the Pt electrodes. For the LiPON modified cells, two Li metal disc electrodes with 2 mm diameter were punched from a 60 µm thick Li foil and pressed onto both surfaces of bare and LiPON-coated Li_6PS_5Cl pellets. The resulting Li/Li_6PS_5Cl/Li and Li/LiPON/Li_6PS_5Cl/LiPON/Li symmetric cells were sealed under vacuum into pouch cells with Cu current collectors. To enhance the contact between the SSE pellets and Li metal anodes, the resulting pouch cells were heated at 80 °C under a stack pressure of 2.3 MPa for 12h. Galvanostatic cycling and EIS measurements were carried out on the two-electrode symmetric cells by cycling at different current densities under a stack pressure of 4.6 MPa at 30 °C on a Biologic multi-channel workstation and Gamry Interface potentiostat, respectively.

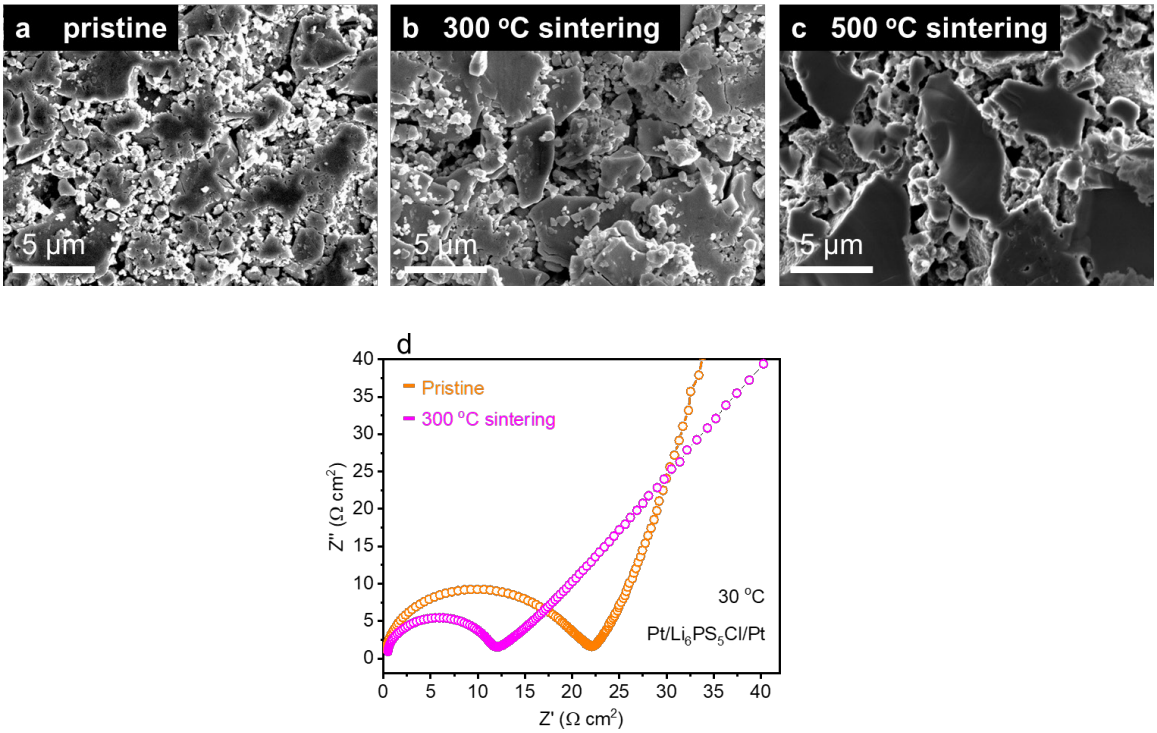

Figure S1. Cross-section SEM images of Li_6PS_5Cl pellets (a) without sintering and sintering at (b) 300 and (c) 500 °C. (d) Comparison of EIS profiles of Pt/Li_6PS_5Cl/Pt symmetric cells made of pristine and 300 °C sintered Li_6PS_5Cl SSE and sputtered Pt electrodes. Compared with the pristine Li_6PS_5Cl SSE, the Li_6PS_5Cl SSE sintered at 300 °C shows a reduced total resistance from 21.9 to 12.0 Ω cm^2, probably because of the improved grain size in the bulk SSE, which is beneficial for impedance reduction and Li ion migration. Even though the Li_6PS_5Cl SSE sintered at 500 °C shows a significantly increased grain size, we found a dramatic decomposition during the sintering process. The fundamental mechanism of the reaction and effect on the performance of Li_6PS_5Cl SSE sintered at high temperature needs to be further investigated, and will be reported in our future papers.

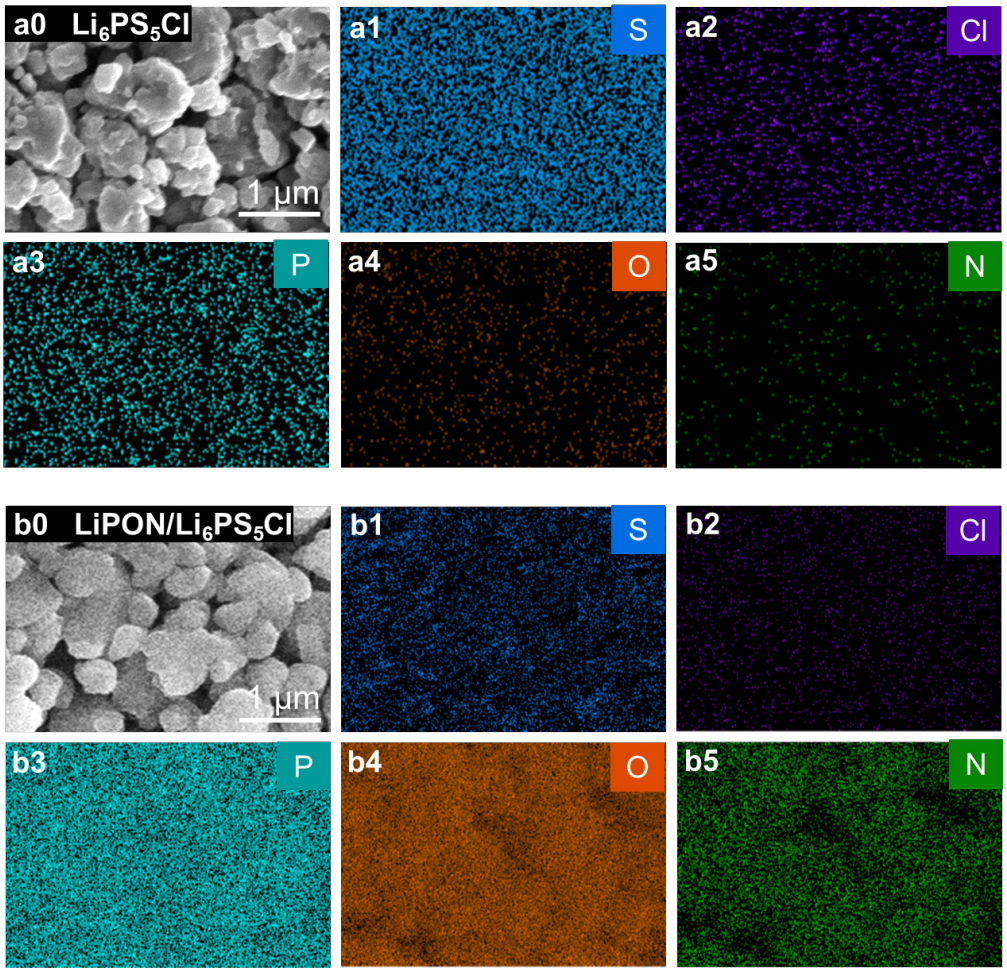

Figure S2. EDX spectroscopy mapping images of (a) bare and (b) LiPON coated Li_6PS_5Cl pellets surface indicating a homogeneous LiPON coating on the Li_6PS_5Cl pellets.

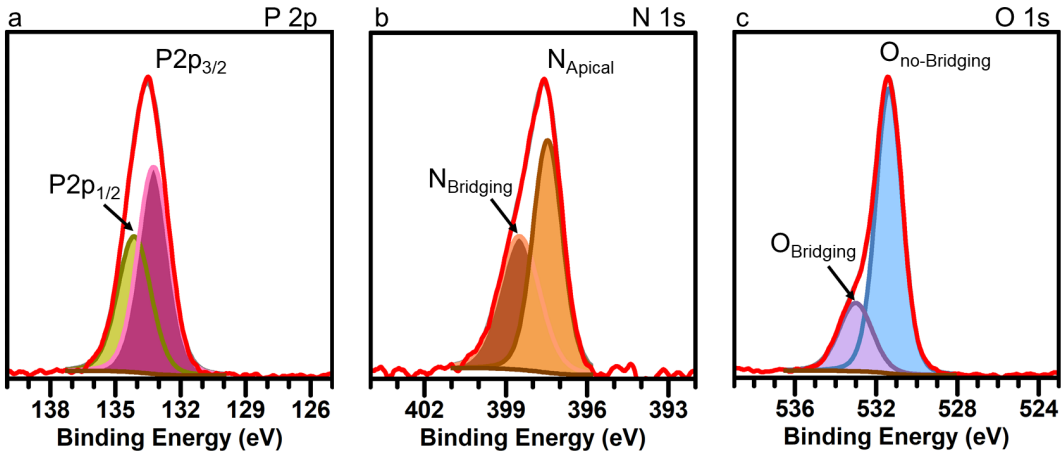

Figure S3. XPS spectra from the surface of LiPON coated Li_6PS_5Cl SSEs for P 2p, N 1s and O 1s regions. The two O 1s peaks arise from non-bridging O at 531.4 eV and bridging O at 532.9 eV. The two peaks from N 1s arise from apical N at 397.5 eV and bridging N at 398.6 eV. The two peaks from P are P $2p_{3/2}$ at 133.3 eV and P $2p_{1/2}$ at 134.0 eV.

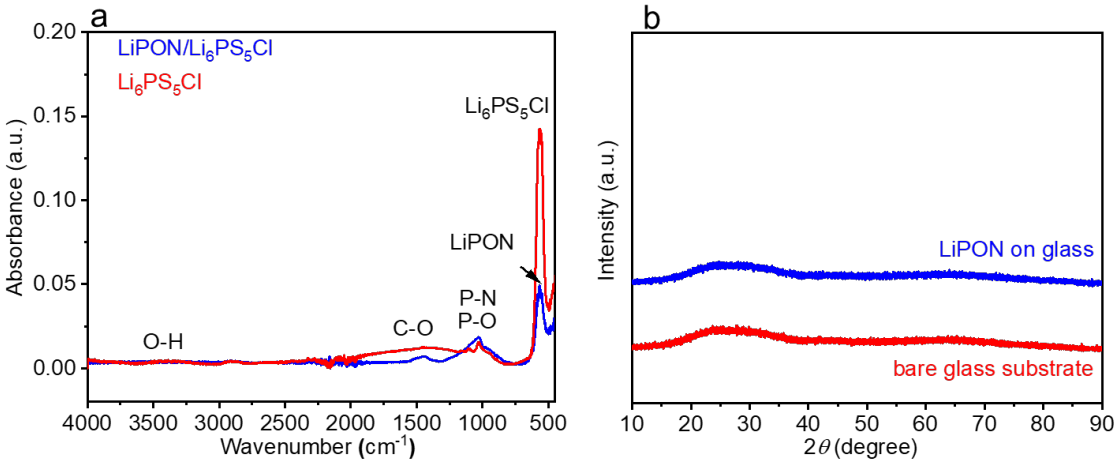

Figure S4. (a) The larger range FTIR spectra of Li_6PS_5Cl SSE with and without LiPON thin-film coating. (b) XRD patterns of LiPON thin-film coated glass and bare glass.

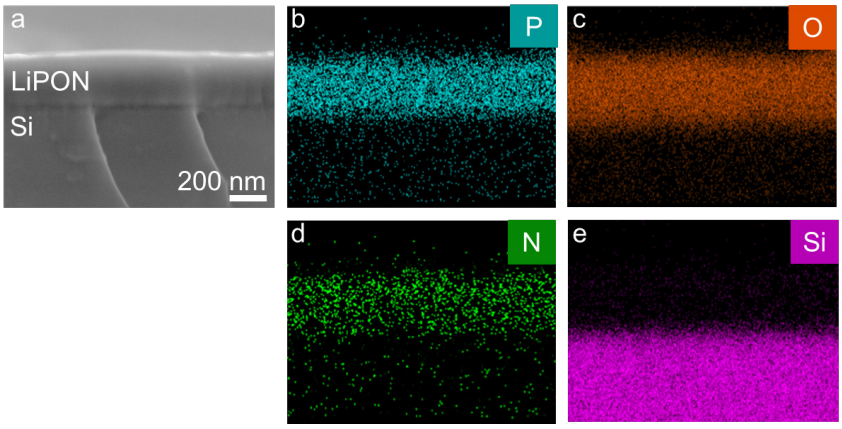

Figure S5. EDX mapping images of LiPON thin-film coated Si.

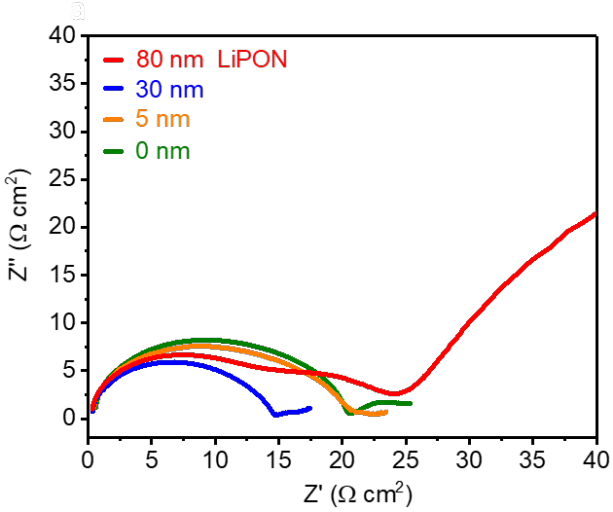

Figure S6. Comparison of EIS profiles of Li/LiPON/Li_6PS_5Cl/LiPON/Li symmetric cells with variety thickness of LiPON interlayers. The cells without and with only 5 nm LiPON interlayer showed a similar total resistance indicating that the 5 nm LiPON interlayer is too thin (or too fragile) to influence the wettability. However, adding an 80 nm LiPON interlayer gave a larger total resistance, indicating 80 nm of LiPON is too thick. The cell with a 30 nm LiPON interlayer showed a much lower total resistance and were chosen for the Li plating/stripping experiments.

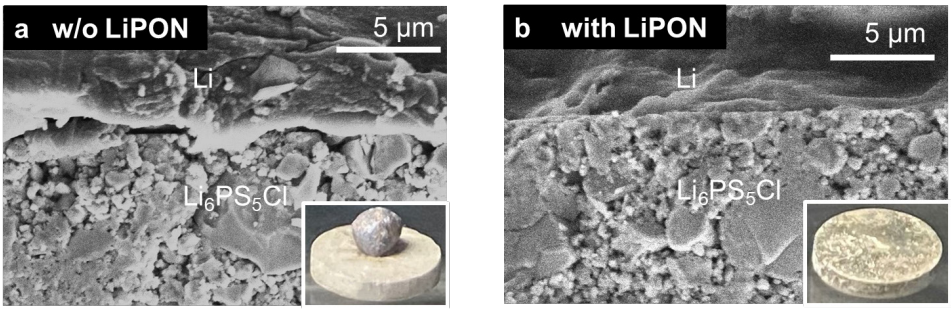

Figure S7. Cross-section SEM images of (a) the bare interface between the Li_6PS_5Cl SSE and Li metal by breaking Li_6PS_5Cl pellet exhibiting interfacial void space between Li_6PS_5Cl SSE and Li metal and (b) the interface between the LiPON coated Li_6PS_5Cl SSE and Li metal showing no interfacial void space between Li_6PS_5Cl SSE and Li metal and is also the evidence of superior interfacial contact. The bottom-right insets are digital photos of (a) a droplet of molten Li formed a ball on the surface of the Li_6PS_5Cl pellet with an obtuse contact angle demonstrating a poor wetting interaction at the bare Li_6PS_5Cl SSE/Li metal interface and (b) molten Li spread out quickly and uniformly covering the surface of the LiPON coated Li_6PS_5Cl pellet with acute angle demonstrates improved wetting behaviour of Li_6PS_5Cl SSE.

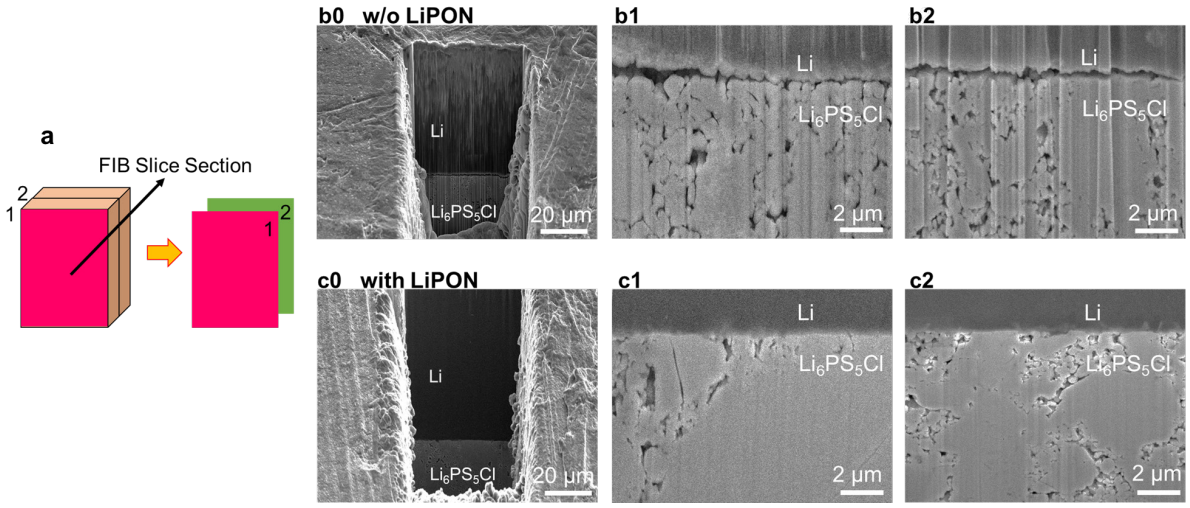

Figure S8. (a) Schematic of the series FIB milling operation to obtain slice SEM images. The series milling slices of FIB-SEM cross-sections images of the Li_6PS_5Cl SSE/Li metal interfaces (b) without and (c) with LiPON coating exhibit a close contact between LiPON coated Li_6PS_5Cl pellet and Li metal interface.

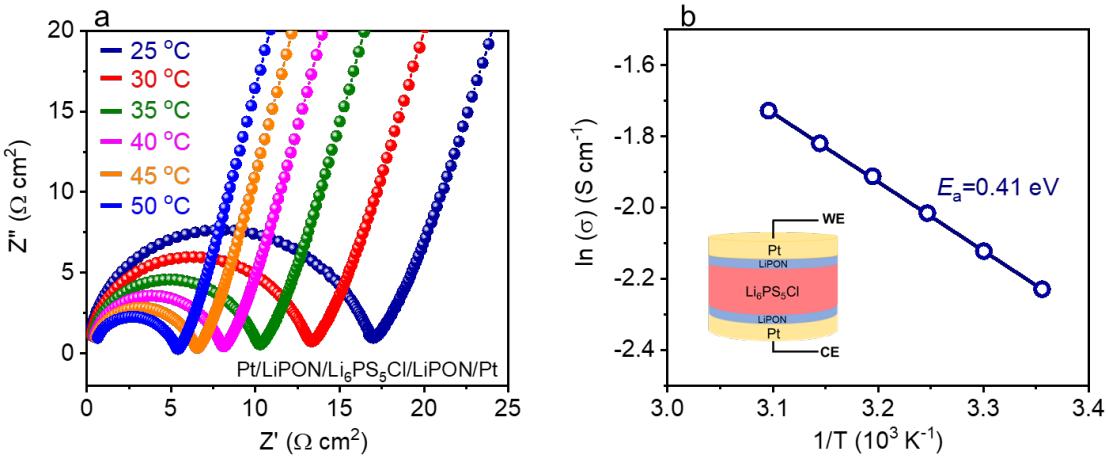

Figure S9. (a) EIS curves of a Pt/LiPON/Li_6PS_5Cl/LiPON/Pt symmetric cell measured at temperatures from 25-50 °C with (b) the corresponding Arrhenius plot of the ionic conductivity.

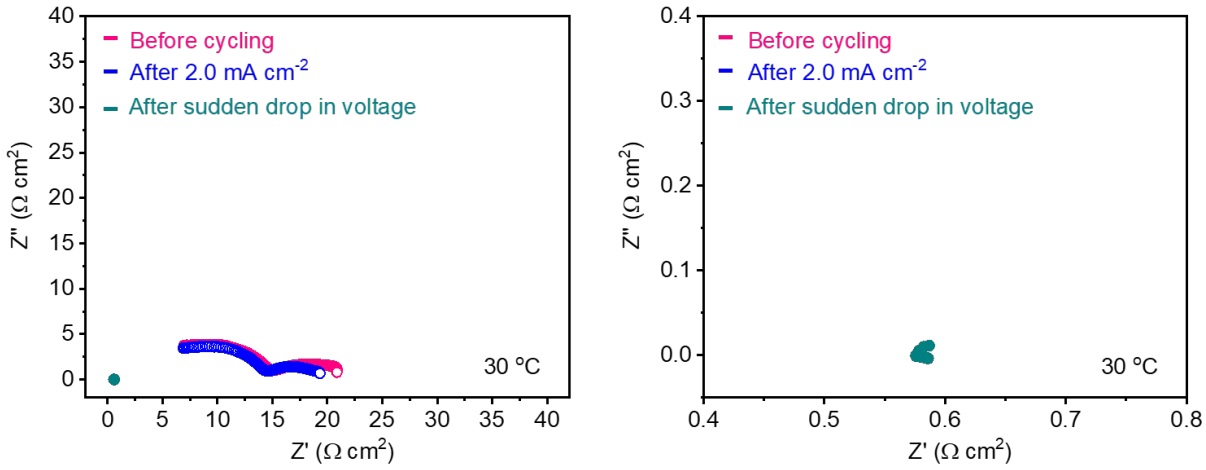

Figure S10. (a) EIS spectra of the Li/LiPON/Li_6PS_5Cl/LiPON/Li symmetric cell before cycling and after applying a current density of 2.0 mA cm^2, and after the voltage sudden drop. (b) Magnified (a) EIS spectra after short-circuiting.

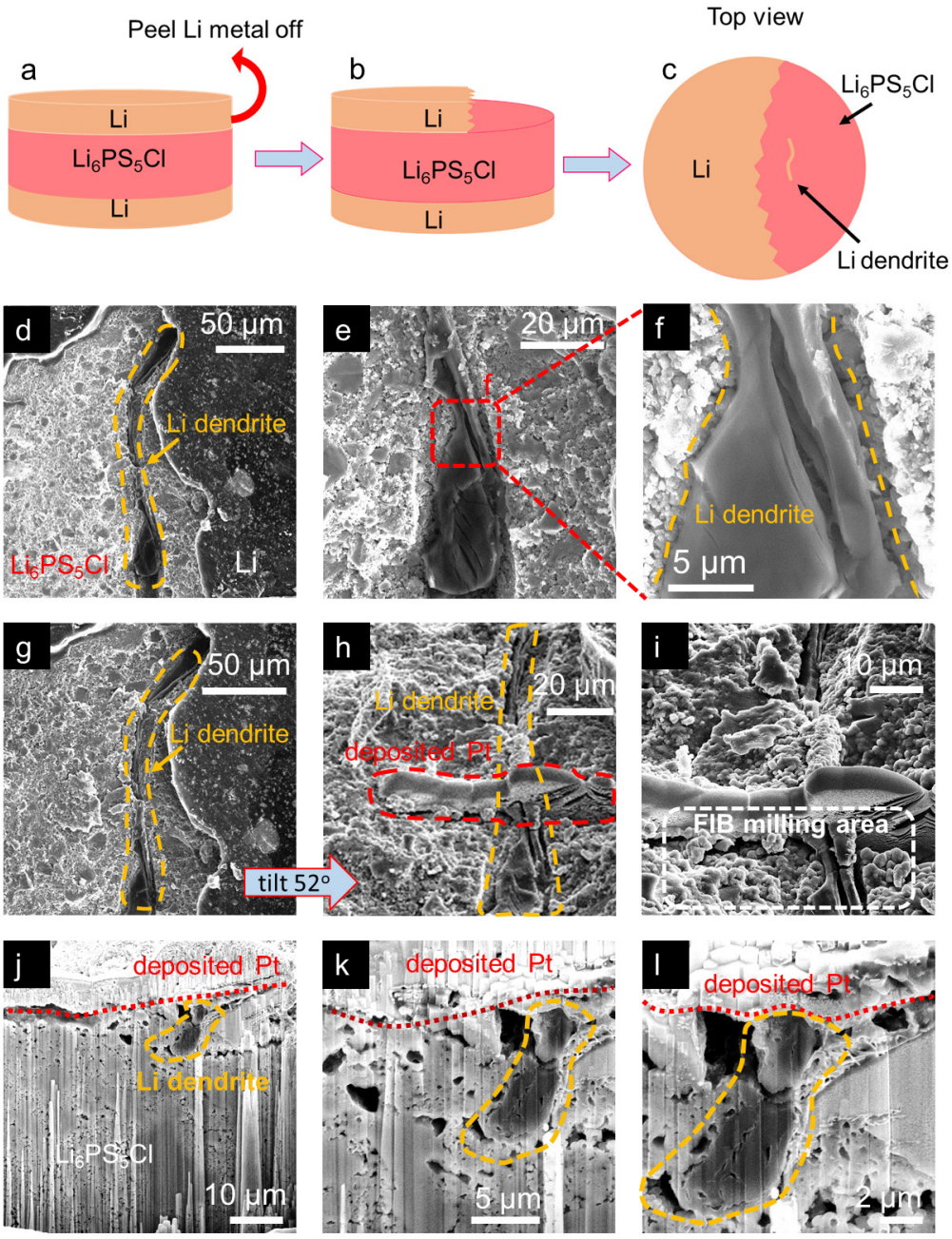

Figure S11. (a-c) Schematic of Li metal peeled from short-circuited Li/Li_6PS_5Cl/Li symmetric cell and the appearance of the Li dendrites. Because excessive peeling operations might crack the pellet, after finding the Li dendrite, we stopped the peeling operation and left some Li metal on the Li_6PS_5Cl SSE surface. (d) Top-view SEM images of Li dendrite growth inside the surface area of Li_6PS_5Cl SSE and (e-f) magnified Li dendrite images. (g-i) Stage tilt, deposition of Pt protection layer before local area milling in the FIB-SEM. (j) FIB-SEM cross-section images of Li dendrite growth inside the surface area and propagation into the bulk of Li_6PS_5Cl SSE and

(k-l) magnified Li dendrite images. This FIB-SEM technique can only look from cross-section of milled slides, and it is difficult to obtain the entire Li dendrite growth topographic morphology in the bulk Li_6PS_5Cl SSE. Although the FIB-SEM images do not show the Li dendrite penetrated the entire electrolyte and connected two electrodes, we have obtained SEM images of Li dendrite growth with ~150 μm length inside the surface and propagation ~10 μm depth to the bulk. We believe that the lithium dendrites had grown through the entire Li_6PS_5Cl SSE because of the cell short-circuiting.

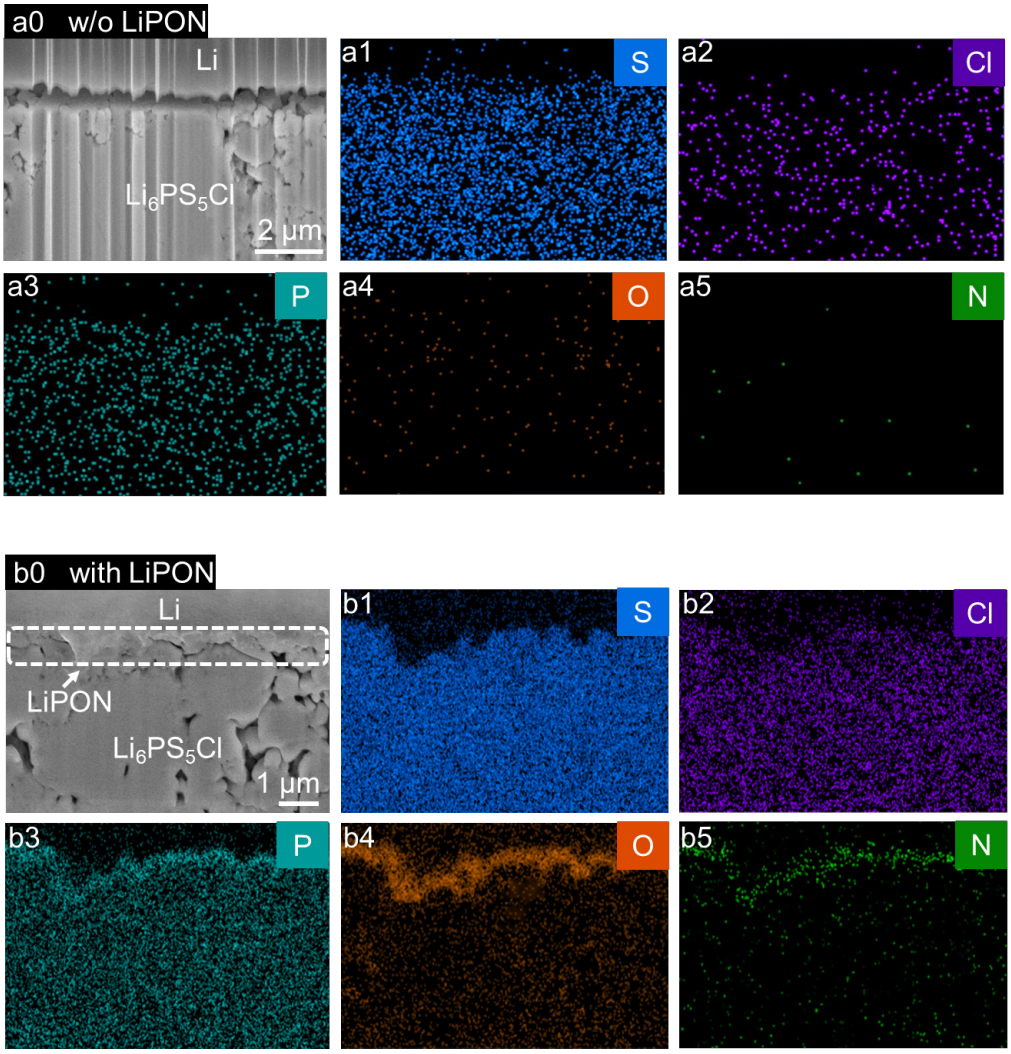

Figure S12. FIB-SEM cross-sectional images of the (a) Li/Li_6PS_5Cl/Li and (b) Li/LiPON/Li_6PS_5Cl/LiPON/Li symmetric cells after cell failure, with corresponding EDX mapping images for S, Cl, P, O, and N.

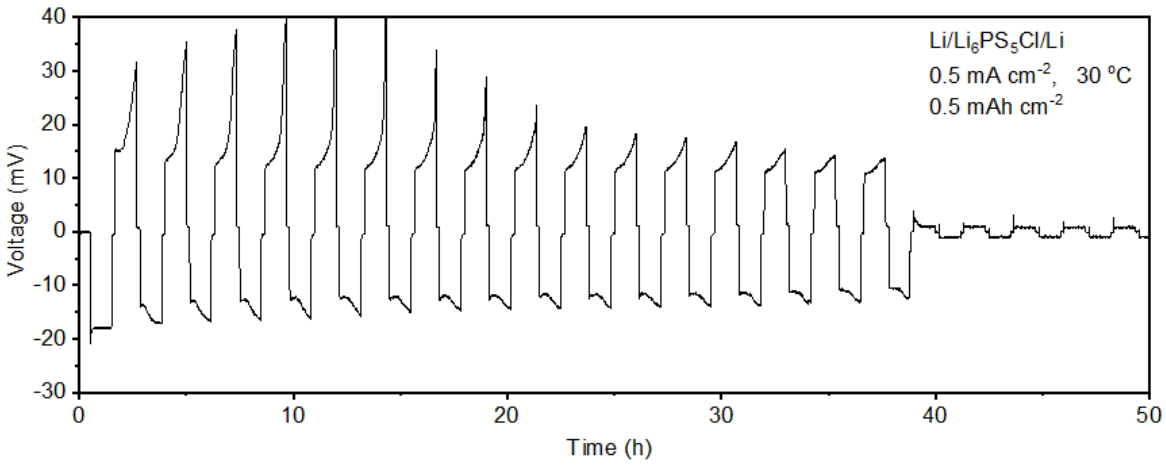

Figure S13. Galvanostatic Li plating/stripping experiment of the symmetric cell without the LiPON thin film coating at a current density of 0.5 mA cm^2 at 30 °C. The noisy potential profile with large voltage polarization demonstrates ununiform Li plating and stripping at the SSE/Li interface leading to the dendrite growth because of the poor contact between SSE and Li metal and the large interfacial resistance.

Table S1. Comparison of critical current densities of this study along with recent reports using argyrodite Li_6PS_5Cl solid-state electrolyte.

Critical current density (mA cm^{-2})	Solid electrolyte materials	Cut-off capacity (mAh cm^{-2})	Test temperature (^{o}C)	Stack pressure (MPa)	Ref.
0.4	Li_6PS_5Cl	0.4	25 ^{o}C	5	1
1.0	Li_6PS_5Cl	1.0	25 ^{o}C	7	2
1.1	Li_6PS_5Cl	0.5	25 ^{o}C	No info.	3
1.5 2.5	Li_6PS_5Cl	1.0	25 ^{o}C 80 ^{o}C	5	4
4.1	Li_6PS_5Cl	0.5	30 ^{o}C	4.6	This work

References

1. C. Hansel and D. Kundu, *Adv Mater Interfaces*, 2021, 8, 2100206.
2. J. Kasemchainan, S. Zekoll, D. S. Jolly, Z. Y. Ning, G. O. Hartley, J. Marrow and P. G. Bruce, *Nat Mater*, 2019, 18, 1105-1111.
3. G. Z. Liu, W. Weng, Z. H. Zhang, L. P. Wu, J. Yang and X. Y. Yao, *Nano Lett*, 2020, 20, 6660-6665.
4. D. S. Jolly, Z. Y. Ning, G. O. Hartley, B. Y. Liu, D. L. R. Melvin, P. Adamson, J. Marrow and P. G. Bruce, *Acs Appl Mater Inter*, 2021, 13, 22708-22716.